A hMTR4-PDIA3P1-miR-125/124-TRAF6 Regulatory Axis and Its Function in NF kappa B Signaling and Chemoresistance

Chen Xie,[1] Li-Zhen Zhang,[2] Zhan-Li Chen,[2] Wang-Jing Zhong,[2] Jian-Hong Fang,[2] Ying Zhu,[2] Man-Huan Xiao,[2] Zhi-Wei Guo,[2] Na Zhao,[2] Xionglei He,[2] and Shi-Mei Zhuang [ID] [1,2]

BACKGROUND AND AIMS: DNA damage-induced NF-κB activation is a major obstacle to effective antitumour chemotherapy. Long noncoding RNAs (lncRNAs) that regulate chemoresistance of cancer cells remain largely unknown. This study aimed to characterize the lncRNAs that may affect chemotherapy sensitivity.

APPROACH AND RESULTS: We found that lncRNA PDIA3P1 (protein disulfide isomerase family A member 3 pseudogene 1) was up-regulated in multiple cancer types and following treatment with DNA-damaging chemotherapeutic agents, like doxorubicin (Dox). Higher PDIA3P1 level was associated with poorer recurrence-free survival of human hepatocellular carcinoma (HCC). Both gain-of-function and loss-of-function studies revealed that PDIA3P1 protected cancer cells from Dox-induced apoptosis and allowed tumor xenografts to grow faster and to be more resistant to Dox treatment. Mechanistically, miR-125a/b and miR-124 suppressed the expression of tumor necrosis factor receptor-associated factor 6 (TRAF6), but PDIA3P1 bound to miR-125a/b/miR-124 and relieved their repression on TRAF6, leading to activation of the nuclear factor kappa B (NF-κB) pathway. Consistently, the effect of PDIA3P1 inhibition in promoting Dox-triggered apoptosis was antagonized by silencing the inhibitor of κBα (IκBα) or overexpressing TRAF6. Administration of BAY 11-7085, an NF-κB inhibitor attenuated PDIA3P1-induced resistance to Dox treatment in mouse xenografts. Moreover, up-regulation of PDIA3P1 was significantly correlated with elevation of TRAF6, phosphorylated p65, or NF-κB downstream antiapoptosis genes in human HCC tissues. These data indicate that enhanced PDIA3P1 expression may confer chemoresistance by acting as a microRNA sponge to increase TRAF6 expression and augment NF-κB signaling. Subsequent investigations into the mechanisms of PDIA3P1 up-regulation revealed that human homologue of mRNA transport mutant 4 (hMTR4), which promotes RNA degradation, could bind to PDIA3P1, and this interaction was disrupted by Dox treatment. Overexpression of hMTR4 attenuated Dox-induced elevation of PDIA3P1, whereas silencing hMTR4 increased PDIA3P1 level, suggesting that Dox may up-regulate PDIA3P1 by abrogating the hMTR4-mediated PDIA3P1 degradation.

CONCLUSION: There exists a hMTR4-PDIA3P1-miR-125/124-TRAF6 regulatory axis that regulates NF-κB signaling and chemoresistance, which may be exploited for anticancer therapy. (Hepatology 2020;71:1660-1677).

Long noncoding RNAs (lncRNAs) are non-protein-coding transcripts of more than 200-nt in length.[1] The function of lncRNAs depends on their subcellular localization.[2] Nuclear lncRNAs may positively or negatively regulate gene expression by binding to DNA, RNA, or proteins and acting

in cis or *in trans*,[3,4] whereas cytoplasmic lncRNAs may modulate posttranslational modification of proteins,[5,6] act as decoys for microRNAs (miRNAs) and proteins,[7] or regulate mRNA stability or translation.[8-10] Growing evidence indicates that lncRNAs are important regulators of different cell activities, and their dysfunction contributes to pathological conditions, such as cancer.

Chemoresistance is a major obstacle to curing cancer. Genotoxic agents, such as doxorubicin (Dox) and etoposide, represent a major class of chemotherapeutic drugs and can induce DNA damage and provoke the nuclear factor kappa B (NF-κB) signaling pathway, resulting in transactivation of potent anti-apoptosis genes (e.g., B-cell lymphoma extra large [Bcl-xL], X-linked inhibitor of apoptosis protein [XIAP], baculoviral IAP [inhibitor of apoptosis protein] repeat-containing protein [BIRC] 2, and BIRC3) and subsequent chemoresistance of cancer cells.[11] Moreover, aberrant NF-κB activation has been observed in multiple cancer types, which provides a rationale for overcoming chemoresistance by targeting the NF-κB pathway. The NF-κB signaling plays important roles in multiple biological processes, including immune response, differentiation, cell survival, proliferation, and migration.[11,12] The core components of the NF-κB pathway include the inhibitor of κB (IκB) proteins, IκB kinase (IKK) complex, and NF-κB dimers. In the "resting" state, NF-κB is associated with IκB proteins and remains inactive in the cytoplasm. Stimulating signals activate the IKK complex, lead to phosphorylation, ubiquitination, and degradation of IκB proteins and in turn nuclear translocation of the NF-κB complex, which consequently transactivates the target genes of NF-κB.[13] Tumor necrosis factor receptor–associated factor (TRAF) family members are obligate signaling intermediates upstream of the IKK complex in the NF-κB pathway. TRAF6 has been shown to induce NF-κB activation in response to a wide variety of stimuli, including cell-surface or intracellular signals and DNA damage.[14,15]

Few lncRNAs have been identified as regulators of the NF-κB pathway. For example, NF-κB-interacting lncRNA (NKILA) binds to NF-κB/inhibitor of κBα (IκBα) and masks the phosphorylation motifs of IκBα, which represses IκBα degradation and NF-κB activation, resulting in increased apoptosis and reduced invasion of MDA-MB-231 cells.[5] lncRNA MIR31HG (miRNA-31 host gene) directly binds to IκBα and promotes its phosphorylation and NF-κB activation, thus inhibiting the differentiation of adipose-derived stem cells into osteoblasts.[16] The lncRNAs Lethe and Carlr interact with the NF-κB subunit p65 and regulate its transcriptional activity.[17]

View this article online at wileyonlinelibrary.com.

Potential conflict of interest: Nothing to report.

ARTICLE INFORMATION:

From the ¹Key Laboratory of Liver Disease of Guangdong Province, the Third Affiliated Hospital, Sun Yat-sen University, Guangzhou, China; ²MOE Key Laboratory of Gene Function and Regulation, School of Life Sciences, Collaborative Innovation Center for Cancer Medicine, Sun Yat-sen University, Guangzhou, China.

ADDRESS CORRESPONDENCE AND REPRINT REQUESTS TO:

Shi-Mei Zhuang, Ph.D., M.D.
School of Life Sciences, Sun Yat-sen University
135 Xingang Xi Road

Guangzhou 510275, China
E-mail: LSSZSM@mail.sysu.edu.cn or zhuangshimei@163.com
Tel.: +86-20-84112164

In an attempt to identify the lncRNAs that regulated chemoresistance of cancer cells, we found that protein disulfide isomerase family A member 3 pseudogene 1 (PDIA3P1), a lncRNA transcript of PDIA3 pseudogene, was up-regulated in various tumors and following treatment with DNA-damaging agents. Subsequent investigations using human hepatocellular carcinoma (HCC) tissues and cell and mouse models revealed that PDIA3P1 up-regulation conferred chemoresistance by acting as a miRNA sponge to increase TRAF6 expression and enhance NF-κB signaling. Furthermore, DNA-damaging agent increased PDIA3P1 level by attenuating human homologue of mRNA transport mutant 4 (hMTR4)-mediated PDIA3P1 degradation. These findings provide insights into the biological function of PDIA3P1, the regulatory network of NF-κB signaling, and the mechanism of chemoresistance and suggest PDIA3P1 as a potential target for cancer therapy.

Materials and Methods

Additional information is provided in the Supporting Materials and Methods. All oligonucleotide sequences are listed in Supporting Table S1.

REAGENTS

The following reagents were used: Dox (HY-15142; MedChemExpress, Monmouth Junction, NJ), etoposide (HY-13629; MedChemExpress), BAY 11-7085 (HY-10257; MedChemExpress), recombinant human interleukin-1β (IL-1β) protein (201-LB-005; R&D Systems, Minneapolis, MN), and tumor necrosis factor α (TNF α) protein (210-TA-010; R&D Systems).

HUMAN TISSUES

HCC and adjacent nontumor liver tissues were collected from patients who underwent HCC resection at Sun Yat-sen University Cancer Center (Guangzhou, China). Both tumor and nontumor tissues were confirmed histologically. No local or systemic treatment had been conducted before surgery. After surgical resection, no other anticancer therapy was administered before relapse. Tissues were immediately snap-frozen in liquid nitrogen until use. Informed consent was obtained from each patient,

and the protocol was approved by the Institutional Research Ethics Committee. Relevant characteristics of the study subjects are summarized in Supporting Table S2.

RNA OLIGORIBONUCLEOTIDES

The following RNA oligoribonucleotides were used: miRNA mimics (hsa-miR-125a-5p, hsa-miR-125b-5p, hsa-miR-124-3p), miR-125a/b inhibitor (anti-miR-125), miR-124 inhibitor (anti-miR-124), and the negative control (NC) of miRNA inhibitor; small interfering RNA (siRNA) targeting PDIA3P1 (siPDIA3P1-1, siPDIA3P1-2), IκBα (siIκBα), TRAF6 (siTRAF6), DROSHA (siDROSHA), DICER1 (siDICER1), hMTR4 (sihMTR4-1, sihMTR4-2), or RRP40 gene (siRRP40); and the NC RNA duplex for siRNA and miRNA.

RAPID AMPLIFICATION OF COMPLEMENTARY DNA ENDS

The 5′ and 3′ end of the PDIA3P1 transcript was determined by the 5′ rapid amplification of complementary DNA ends (RACE) and 3′ RACE System, respectively (Version 2.0; Invitrogen, Carlsbad, CA) using total RNA from normal liver tissues.

PLASMID CONSTRUCTION

Lentivirus expression vectors pCDH-PDIA3P1, pCDH-S1m-PDIA3P1, pCDH-S1m-PDIA3P1-mut (mutant), pCDH-shNC, pCDH-shPDIA3P1, pCDH-TRAF6, and pCDH-hMTR4 were generated using pCDH-CMV-MCS-EF1-copGFP (copepod green fluorescent protein) (System Biosciences, Palo Alto, CA), which contained a copGFP expression cassette and was designated as pCDH-Ctrl (control) in this study. pc3-gab-PDIA3P1 was generated using pc3-gab,[18] in which the neomycin in pcDNA3.0 vector (Invitrogen) was replaced with the enhanced green fluorescent protein. Luciferase reporter vectors pGL3cm-PDIA3P1, pGL3cm-PDIA3P1-125M, pGL3cm-PDIA3P1-124M, and pGL3cm-TRAF6-3′ untranslated region (UTR) were generated using pGL3cm vector,[18] which was produced based on pGL3-control (Promega, Madison, WI). pGL3-basic-p-(−2,129/+358) was constructed based on pGL3-basic vector (Promega).

LENTIVIRUS PRODUCTION

For lentivirus production, the lentivirus expression vector that contained the target sequence was co-transfected into human embryonic kidney (HEK) 293T cells with the packaging plasmid mix (Lenti-X HTX Packaging Mix; Clontech, Palo Alto, CA) by calcium phosphate precipitation. The lentivirus supernatant was harvested and stored in aliquots at –80°C until use.

CELL LINES

The human hepatoma cell lines, SK-Hep-1 and QGY-7703, were cultured in Dulbecco's modified Eagle's medium (Life Technologies, Carlsbad, CA), supplemented with 10% fetal bovine serum (HyClone, Logan, UT), 100 U/mL penicillin, and 100 μg/mL streptomycin in a humidified atmosphere of 5% CO_2 at 37°C.

The stable cell lines were established by infecting SK-Hep-1 or QGY-7703 cells with lentivirus that expressed the target sequence and selected by puromycin treatment. Sublines with stable expression of PDIA3P1 (SK-PDIA3P1, QGY-PDIA3P1), S1m-tagged wild-type PDIA3P1 (QGY-S1m-PDIA3P1), S1m-tagged PDIA3P1 with mutant miR-125a/b-binding sites and miR-124-binding sites (QGY-S1m-PDIA3P1-mut), TRAF6 (SK-TRAF6, QGY-TRAF6) or hMTR4 (QGY-hMTR4) and their control lines (SK-Ctrl, QGY-Ctrl), as well as QGY-shPDAI3P1 with stable silencing of PDAI3P1 and its control line QGY-shNC, were constructed. All sublines expressed copGFP.

CELL TRANSFECTIONS

Cells were transfected with RNA oligoribonucleotides using Lipofectamine RNAiMAX (Invitrogen). The final concentrations of RNA duplex and miRNA inhibitor were 50 nM and 200 nM, respectively. Transfection with plasmid DNA alone or together with RNA duplex was performed using Lipofectamine 2000 (Invitrogen).

ANALYSIS OF GENE EXPRESSION

The expression level of target genes was analyzed by real-time quantitative PCR, western blotting, or immunohistochemical staining.

LUCIFERASE REPORTER ASSAY

Luciferase activity was measured using the dual-luciferase reporter assay system (Promega). *Renilla* luciferase expressed by pRL-PGK (Promega) was used as an internal control to correct for differences in both transfection and harvest efficiency.

To examine the activity of NF-κB signaling, a luciferase reporter plasmid containing the minimal promoter with multiple tandem NF-κB-binding sites (pNF-κB-Luc; Clontech) was used. Cells were transfected with 50 nM RNA duplex for 24 hours and then co-transfected with 50 ng pNF-κB-Luc and 2 ng pRL-PGK for 32 hours, followed by Dox treatment for 12 hours before the luciferase activity assay.

To verify the target genes of miRNAs, cells were co-transfected with 50 nM miRNAs or NC duplex, 2 ng pRL-PGK, and 20 ng firefly luciferase reporter plasmid that contained the wild-type or mutant miRNA-binding sequence of the target gene for 48 hours.

To test the competing endogenous RNA (ceRNA) activity of PDIA3P1 with the luciferase reporter system, SK-PDIA3P1, SK-Ctrl, QGY-PDIA3P1, or QGY-Ctrl cells were co-transfected with 10 nM RNA duplex, 2 ng pRL-PGK, and 10 ng pGL-3cm-TRAF6-3′ UTR.

To characterize the PDIA3P1 promoter, cells were co-transfected with 2 ng pRL-PGK and 100 ng pGL3-basic-p-(–2,129/+358) for 48 hours.

ISOLATION OF CYTOPLASMIC AND NUCLEAR FRACTION

The cytoplasmic and nuclear extracts were isolated using NE-PER Nuclear and Cytoplasmic Extraction Reagents (Pierce, Rockford, IL). The RNAs and proteins from cytoplasmic and nuclear fraction were extracted and examined by real-time quantitative PCR and western blotting, respectively.

IMMUNOFLUORESCENT STAINING FOR p65

The cells were fixed by 4% paraformaldehyde and stained with rabbit monoclonal antibody against p65, followed by incubation with HiLyte Fluor 555-conjugated goat antirabbit immunoglobulin G (IgG) (28176-05-H555; AnaSpec, Fremont, CA) and nuclear counterstaining with 4′,6′-diamidino-2-phenylindole (DAPI) (Sigma-Aldrich, St. Louis, MO).

ANALYSIS OF CELL APOPTOSIS

Apoptosis was evaluated by morphological examination, caspase-3 detection, and annexin V staining. For morphological examination, cells were stained with DAPI, and those with condensed or fragmented nuclei were considered apoptotic cells. At least 500 cells were counted for each sample. Caspase-3 was detected by immunoblotting using rabbit polyclonal antibody against caspase-3 for active caspase-3 (17/19 kDa) and pro-caspase-3 (35 kDa). The annexin V/propidium iodide (PI) assay was conducted using an annexin V-fluorescein isothiocyanate (FITC)/PI Apoptosis Detection Kit (Bimake, Houston, TX) followed by flow cytometry analysis.

MOUSE XENOGRAFT MODELS

Male nonobese diabetic protein kinase, DNA-activated, catalytic polypeptide (Prkdc)^{em26Cd52}Il2rg^{em26Cd22}/Nju (NCG) mice at 4 to 5 weeks of age were used.

For loss-of-function study, QGY-shPDIA3P1 and QGY-shNC cells (2.5×10^6) were resuspended in 75 μL of Matrigel (3432-005-01; R&D Systems) and then subcutaneously injected into either side of the posterior flank of the same mouse. A total of 14 mice were included. Ten days after implantation, when tumor volume reached approximately 50 mm^3, vehicle (1× phosphate-buffered saline [PBS], intravenously) or Dox (3 mg/kg, intravenously) was administered through the caudal vein twice a week for a total of 7 times. Mice were sacrificed 33 days after implantation.

For gain-of-function study, QGY-PDIA3P1 or QGY-Ctrl cells (2×10^6) were resuspended in 75 μL of Matrigel and then subcutaneously injected into either side of the posterior flank of the same mouse. A total of 33 mice were included. Ten days after implantation, vehicle (1× PBS, intravenously; corn oil, intraperitoneally), Dox (3 mg/kg, intravenously), or combined BAY 11-7085 (5 mg/kg, intraperitoneally) and Dox (3 mg/kg, intravenously) was administered twice a week for a total of 4 times. Mice were sacrificed 24 days after implantation.

Tumor growth was monitored every 3 days, and the volume of tumor was measured with calipers and calculated as follows: volume = length × width^2/2. At the end of experiments, tumors were harvested, photographed, and weighed. Aliquots of tumor tissues were freshly frozen in liquid nitrogen and fixed in 10% formalin and embedded in paraffin.

All mouse experiments were approved by the Institutional Animal Care and Use Committee at Sun Yat-sen University. All procedures for animal experiments were performed in accordance with the Guide for the Care and Use of Laboratory Animals (NIH publications 80-23, revised 1996) and according to the institutional ethical guidelines for animal experiments.

RNA IMMUNOPRECIPITATION ASSAY

RNA immunoprecipitation (RIP) assay was used to investigate the interaction between RNA and protein. The argonaute 2 (AGO2) and hMTR4 RNA complexes were respectively immunoprecipitated by anti-AGO2 and anti-hMTR4 antibody. The isotype-matched IgG was used as a negative control. RNA was extracted from the precipitates by TRIzol reagent (Invitrogen).

S1m-TAGGED RNA AFFINITY PURIFICATION

PDIA3P1-interacted RNA was identified by S1m-tagged RNA affinity purification. S1m-PDIA3P1 or S1m-PDIA3P1-mut and their binding RNAs were pulled down by streptavidin Dynabeads (65001; Invitrogen), and the untagged PDIA3P1 was used as a negative control. RNA was extracted from the precipitates by TRIzol reagent.

RNA PULL-DOWN ASSAY

RNA pull-down assay was performed using *in vitro* transcribed biotinylated RNA and streptavidin Dynabeads. The retrieved proteins were separated by sodium dodecyl sulfate-polyacrylamide gel electrophoresis and analyzed by mass spectrometry (Beijing Protein Innovation, Beijing, China) or western blotting.

STATISTICAL ANALYSIS

The difference in PIDA3P1 expression between the paired HCC tissues and adjacent nontumor liver tissues was analyzed with a paired Student t test. Recurrence-free survival (RFS) was calculated from the date of HCC resection to the time of first recurrence. Patients who were lost to follow-up or who died from causes

unrelated to HCC were treated as censored data. Kaplan-Meier survival curves and Cox proportional hazard regression analyses were performed using SPSS version 16.0 software (IBM SPSS, Inc., Chicago, IL).

Data are expressed as the mean ± SEM of at least three independent experiments. Unless otherwise noted, the differences between groups were analyzed using Student t test when only two groups were compared or one-way analysis of variance followed by Dunnett's test when more than two groups were compared. A P value of less than 0.05 was considered the criterion of statistical significance, and all statistical tests were two-sided. All analyses were performed using GraphPad Prism version 5.0 software (GraphPad Software, Inc., San Diego, CA).

Results

PDIA3P1 IS UP-REGULATED BY DNA-DAMAGING AGENTS AND INHIBITS APOPTOSIS BY REGULATING THE NF-κB PATHWAY

To identify lncRNA candidates that may affect the sensitivity of tumor cells to chemotherapy, a bioinformatics analysis was conducted based on the transcriptome profiles (accession number: GSE43541, GSE58074, GSE32301, GSE42531, GSE63351) of various tumor cells treated with Dox, a commonly used chemotherapeutic drug that causes DNA damage. PDIA3P1, a lncRNA transcript of PDIA3 pseudogene located on chromosome 1q21.1, was the only lncRNA up-regulated by Dox in all five data sets (Supporting Fig. S1A,B). We further validated that Dox treatment up-regulated PDIA3P1 expression in a dose-dependent and time-dependent manner using two hepatoma cell lines, SK-Hep-1 and QGY-7703 (Fig. 1A; Supporting Fig. S2A,B). Consistently, exposure to etoposide, another DNA-damaging agent, also induced PDIA3P1 expression (Fig. 1B; Supporting Fig. S2C), suggesting that PDIA3P1 may be up-regulated by DNA-damaging agents.

Gene Ontology analysis revealed that the protein-coding genes co-expressed with PDIA3P1 were enriched in the NF-κB pathway (Supporting Fig. S3).

It is well known that DNA-damaging agents can activate NF-κB signaling. We therefore explored whether PDIA3P1 affected the Dox-triggered NF-κB activation using two siRNAs that significantly reduced the expression of PDIA3P1 but did not change the mRNA or protein level of its parental gene PDIA3 (Supporting Fig. S4A-D). Notably, silencing PDIA3P1 abrogated the Dox-induced activation of the NF-κB reporter (Fig. 1C; Supporting Fig. S5A), attenuated the enhanced phosphorylation of IKKα/β, IκBα, and NF-κB/p65 (Fig. 1D) and nuclear translocation of NF-κB/p65 (Fig. 1E; Supporting Fig. S5B) in the cells treated with Dox and two classical NF-κB activators, IL-1β and TNFα. Consistently, knockdown of PDIA3P1 impeded the Dox-induced transactivation of NF-κB downstream anti-apoptosis genes, such as Bcl-xL, XIAP, and BIRC3 (Fig. 1F), and promoted Dox-induced apoptosis (Fig. 2A; Supporting Fig. S5C,D). In contrast, ectopic expression of PDIA3P1 (Supporting Fig. S6A-D) attenuated Dox-stimulated apoptosis (Fig. 2B; Supporting Fig. S7). Moreover, knockdown of IκBα, the inhibitor of NF-κB, significantly abolished the pro-apoptosis effect of siPDIA3P1 (Fig. 2C). These findings imply that PDIA3P1 may repress apoptosis by promoting NF-κB signaling, and silencing PDIA3P1 may sensitize tumor cells to DNA-damaging agents.

PDIA3P1 IS UP-REGULATED IN CANCER TISSUES AND CONFERS TUMOR XENOGRAFTS WITH RESISTANCE TO DNA-DAMAGING AGENT

The biological significance of PDIA3P1 was then investigated using human HCC tissues and mouse xenograft models. The results showed that PDIA3P1, but not its parental gene PDIA3, was up-regulated in HCC tissues (Fig. 3A). Analysis of the transcriptome data from The Cancer Genome Atlas revealed that PDIA3P1 up-regulation was common in different malignancies (Supporting Fig. S8A). Further investigations identified a significant correlation between the level of PDIA3P1 and the expression of NF-κB downstream anti-apoptosis genes XIAP and BIRC2 in tumor tissues (Supporting Fig. S8B). Kaplan-Meier survival analysis revealed that higher PDIA3P1 level was associated with shorter RFS of HCC patients
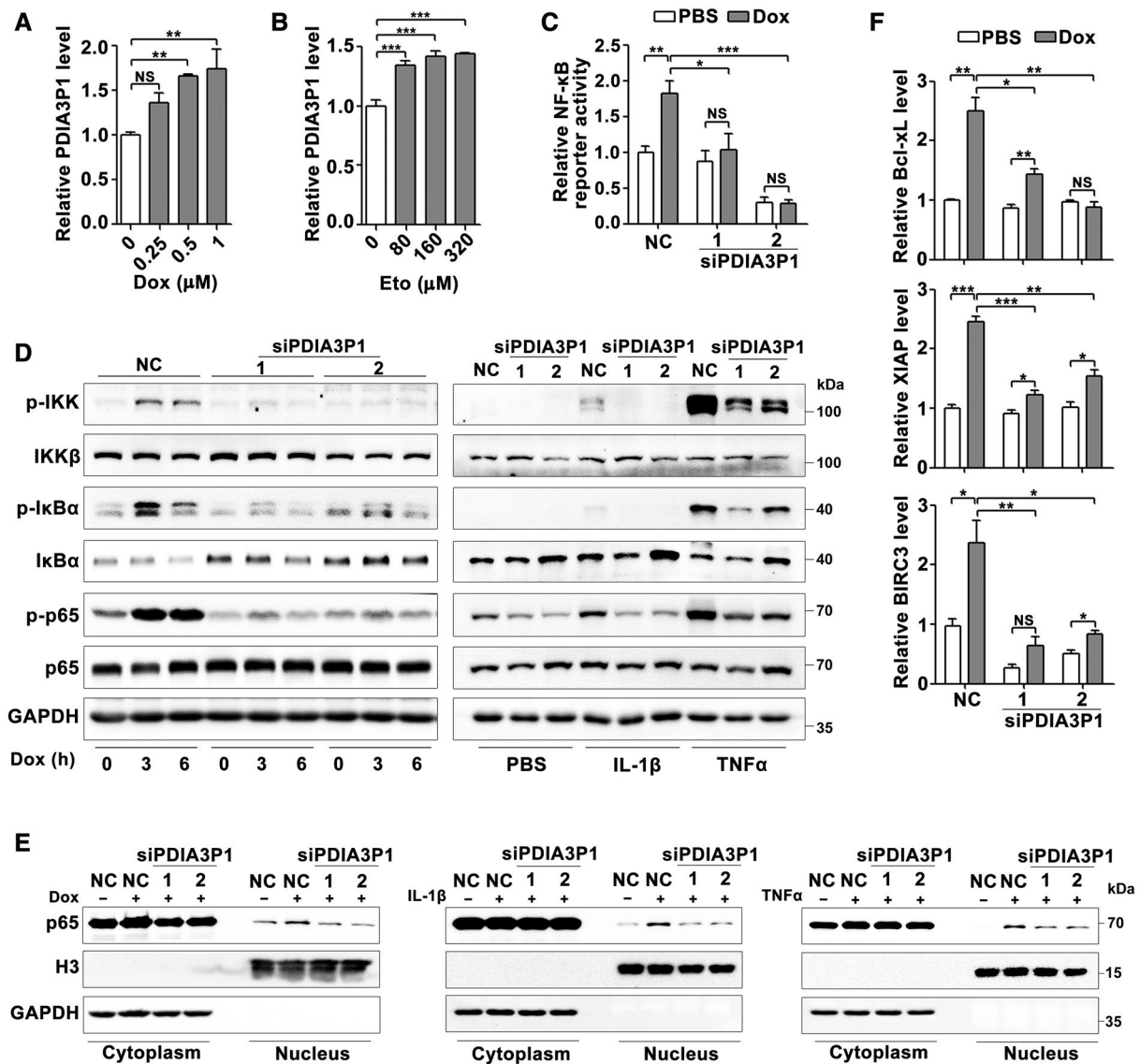
FIG. 1. PDIA3P1 expression is induced by Dox treatment, and silencing PDIA3P1 abrogates Dox-activated NF-κB signaling. (A,B) Dox and etoposide induced PDIA3P1 expression in a dose-dependent manner. SK-Hep-1 cells were treated with the indicated dose of Dox (A) or etoposide (B) for 12 hours and then subjected to real-time quantitative PCR analysis. (C) PDIA3P1 knockdown reduced Dox-induced NF-κB reporter activity. SK-Hep-1 cells transfected with NC or siPDIA3P1-1 or siPDIA3P1-2 for 24 hours were then co-transfected with pNF-κB-Luc and pRL-PGK, followed by incubation with vehicle (PBS) or 0.5 μM Dox for 12 hours before luciferase activity analysis. (D) Silencing of PDIA3P1 attenuated the Dox-, IL-1β-, or TNFα-stimulated phosphorylation of IKK, IκBα, and NF-κB/p65. NC or siPDIA3P1- transfected SK-Hep-1 cells were treated with 1 μM Dox for the indicated time (left panel), or exposed to vehicle (PBS) or 10 ng/mL IL-1β for 7.5 minutes, or 5 ng/mL TNFα for 5 minutes (right panel) before immunoblotting. (E) PDIA3P1 knockdown blocked the Dox-, IL-1β-, or TNFα-stimulated nuclear translocation of p65/NF-κB. NC or siPDIA3P1-transfected SK-Hep-1 cells were treated with 1 μM Dox for 12 hours, or 20 ng/mL IL-1β or TNFα for 10 minutes before isolation of cell fraction and immunoblotting. + or – indicates cells with (+) or without (–) the indicated treatment. GAPDH and histone 3 (H3) were used as the controls for cytoplasmic and nuclear proteins, respectively. (F) PDIA3P1 knockdown suppressed Dox-induced expression of NF-κB target genes. NC or siPDIA3P1-transfected SK-Hep-1 cells were incubated in the presence of vehicle (PBS) or 0.5 μM Dox for 30 hours before real-time quantitative PCR analysis. For (A)-(D) and (F), GAPDH was used as an internal control. For (A)-(C) and (F), data are expressed as the mean ± SEM of at least three independent experiments. $*P < 0.05$; $**P < 0.01$; $***P < 0.001$. Abbreviations: Eto, etoposide; and NS, not significant.
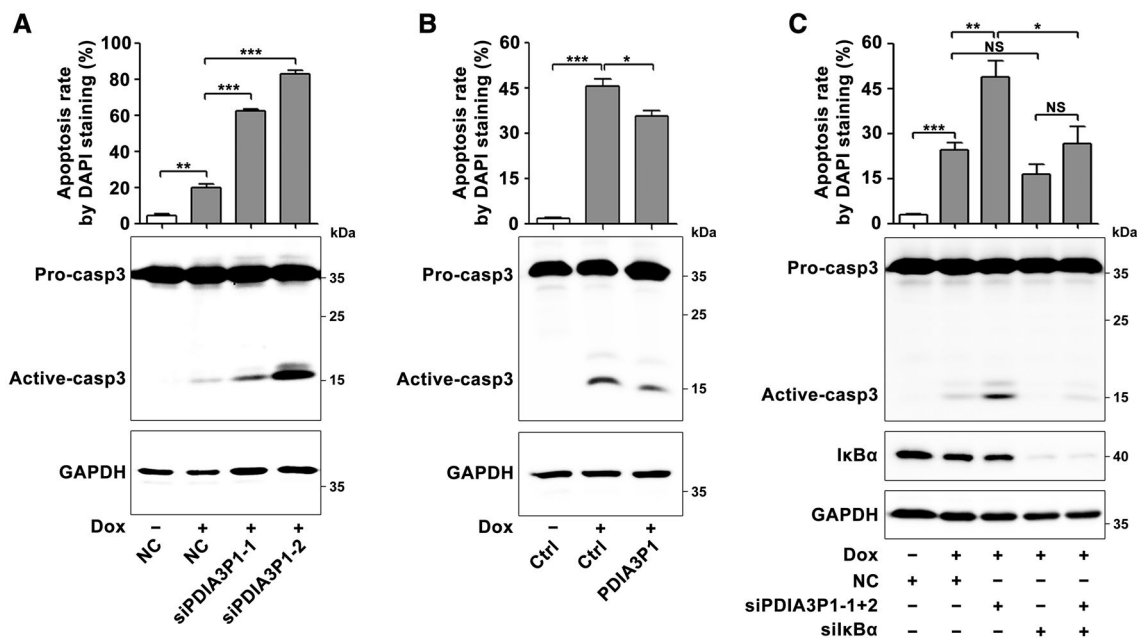
FIG. 2. PDIA3P1 inhibits Dox-induced apoptosis. (A) PDIA3P1 knockdown sensitized cancer cells to Dox-induced apoptosis. NC or siPDIA3P1-transfected SK-Hep-1 cells were treated with 0.25 µM Dox for 48 hours before DAPI staining or for 36 hours before immunoblotting. (B) Ectopic expression of PDIA3P1 inhibited Dox-induced apoptosis. SK-PDIA3P1 and its control line SK-pCDH-Ctrl were treated with 1 µM Dox for 48 hours before DAPI staining or for 42 hours before immunoblotting. (C) IκBα knockdown abrogated the pro-apoptosis effect of PDIA3P1 silencing. SK-Hep-1 cells co-transfected with the indicated siRNA duplexes were treated with 0.25 µM Dox for 36 hours before DAPI staining or for 30 hours before immunoblotting. GAPDH was used as an internal control; + or − indicates cells with (+) or without (−) the indicated treatment. Data are expressed as the mean ± SEM of at least three independent experiments. *$P < 0.05$; **$P < 0.01$; ***$P < 0.001$.

(Fig. 3B), and both univariate and multivariate analyses confirmed PDIA3P1 up-regulation as an independent risk factor for poorer RFS (Supporting Table S2).

Next, mouse models were applied to evaluate whether PDIA3P1 affected the sensitivity of hepatoma to Dox treatment. As shown, PDIA3P1 silencing moderately reduced xenograft growth, and the combination of siPDIA3P1 and Dox treatment exerted a more prominent growth inhibitory effect on hepatoma xenografts compared with Dox treatment or PDIA3P1 silencing alone (Fig. 3C; Supporting Fig. S9A,B). On the other hand, enhanced PDIA3P1 expression allowed xenografts to grow faster, have more nuclear translocation of NF-κB/p65, and be more resistant to Dox treatment, whereas administration of BAY 11-7085, an inhibitor of IκBα phosphorylation, attenuated the PDIA3P1-induced NF-κB/p65 nuclear translocation and chemoresistance (Fig. 3D; Supporting Fig. S9C; Supporting

Fig. S10A,B). Collectively, these data indicate that up-regulation of PDIA3P1 may desensitize tumor cells to chemotherapy.

PDIA3P1 PROMOTES NF-κB ACTIVATION AND TUMOR CELL SURVIVAL BY ACTING AS A MIRNA SPONGE TO UP-REGULATE TRAF6 EXPRESSION

Next, the mechanism by which PDIA3P1 exerted its function was elucidated. We have shown that silencing PDIA3P1 abrogated the Dox, IL-1β, or TNFα-enhanced phosphorylation of IKKα/β, IκBα, and NF-κB/p65 (Fig. 1D). Therefore, the key regulators upstream of IKKα/β in both DNA damage-activated and cytokine-activated NF-κB signaling,[15] such as TRAF6, NF-κB essential modulator (NEMO), transforming growth factor β-activated
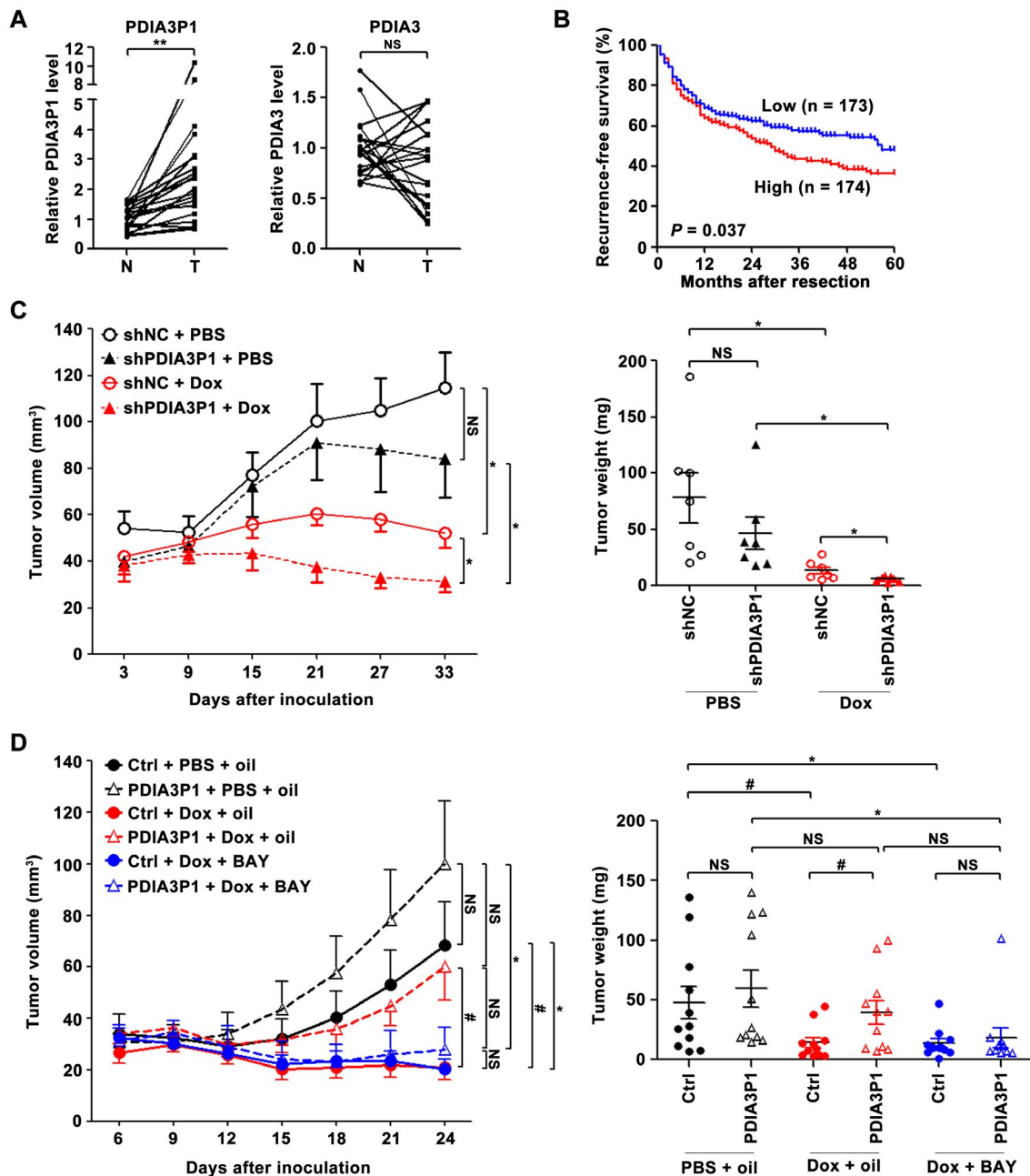
FIG. 3. PDIA3P1 is up-regulated in HCC tissues and confers tumor xenografts with resistance to Dox treatment. (A) PDIA3P1 expression was significantly increased in HCC tissues. The expression of PDIA3P1 or its parental gene PDIA3 was assessed by real-time quantitative PCR in 20 paired HCC (T) and adjacent nontumor liver tissues (N). U6 was used as an internal control. (B) Kaplan-Meier analysis revealed an association between a higher PDIA3P1 level and a shorter RFS. The median PDIA3P1 level in all 347 cases examined was chosen as the cut-off value for separating the PDIA3P1 high-level group (n = 174) from the PDIA3P1 low-level group (n = 173). (C) Silencing of PDIA3P1 sensitized tumors to Dox treatment. NCG mice bearing QGY-shPDIA3P1 and QGY-shNC xenografts were injected with Dox or vehicle (PBS). Seven mice were used for each group. (D) PDIA3P1 overexpression desensitized tumors to Dox treatment. NCG mice bearing QGY-PDIA3P1 and QGY-Ctrl xenografts were injected with vehicle (PBS and corn oil), Dox, or combined Dox and BAY 11-7085. Eleven mice were used for each group. For (C) and (D), the curve of tumor growth and the weight of dissected tumors are shown. [#]$P < 0.05$ for "PDIA3P1 + Dox + oil" or "Ctrl + PBS + oil" versus "Ctrl + Dox + oil." [*]$P < 0.05$; [**]$P < 0.01$.

kinase 1 (TAK1), and TAK1-binding protein 3 (TAB3), were examined. As shown, PDIA3P1 knockdown significantly decreased the protein but not mRNA level of TRAF6 (Fig. 4A; Supporting Fig. S11A) and did not affect the levels of NEMO, TAK1, and TAB3 proteins in cells exposed to vehicle, Dox, IL-1β, or TNFα (Supporting Fig. S11B,C). Consistently, ectopic expression of PDIA3P1 increased the protein level of TRAF6 (Fig. 4B). Moreover, the xenografts of shPDIA3P1 transfectants displayed much lower levels of TRAF6 (Fig. 4C; Supporting Fig. S11D,E). Similar to the effects of PDIA3P1 silencing (Fig. 1C), TRAF6 knockdown attenuated Dox-induced NF-κB reporter activity and increased Dox-induced apoptosis (Supporting Fig. S12A,B). Moreover, TRAF6
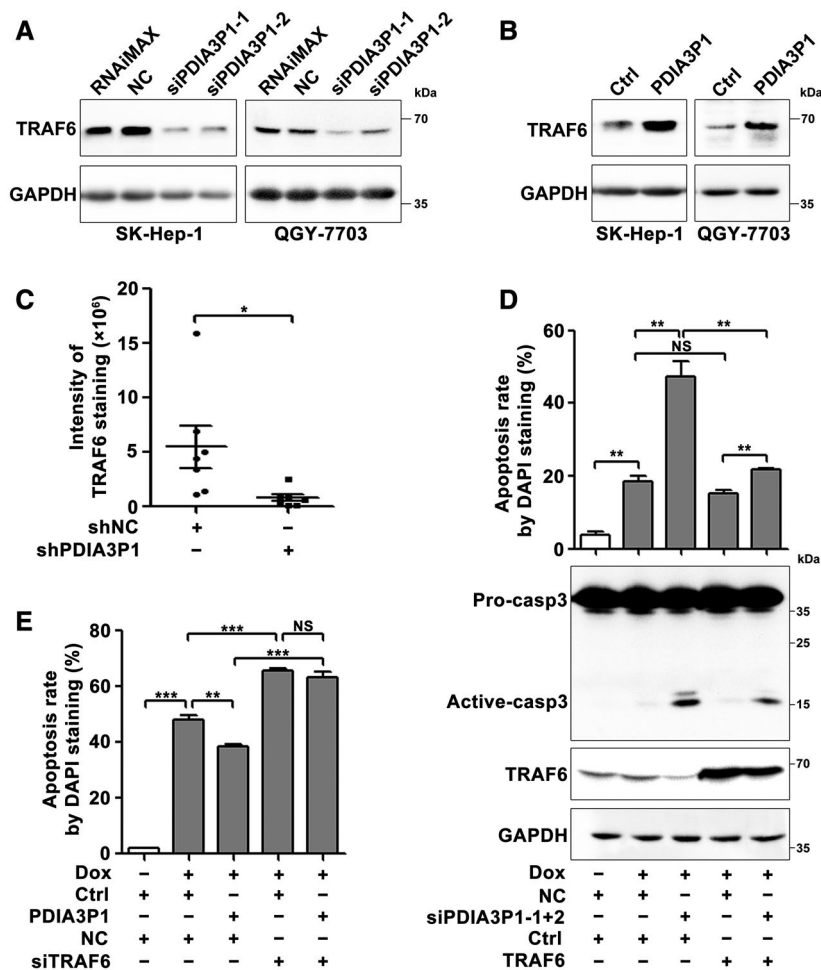

FIG. 4. PDIA3P1 inhibits apoptosis by enhancing TRAF6 expression. (A) PDIA3P1 knockdown reduced the protein level of TRAF6. SK-Hep-1 or QGY-7703 cells were transfected with the indicated RNA duplexes for 48 hours before immunoblotting. RNAiMAX indicates cells exposed to Lipofectamine RNAiMAX but not RNA duplexes. (B) Ectopic expression of PDIA3P1 increased the protein level of TRAF6. SK-Hep-1 or QGY-7703 cells were transfected with pc3-gab-PDIA3P1 (PDIA3P1) or its control pc3-gab (Ctrl) plasmid for 48 hours before western blotting. (C) The xenografts of shPDIA3P1 transfectants displayed lower levels of TRAF6. The intensity of TRAF6 immunohistochemical staining was analyzed. (D) Overexpression of TRAF6 abrogated the promotive effect of siPDIA3P1 on Dox-induced apoptosis. SK-TRAF6 and its control cell line SK-Ctrl were transfected with NC or siPDIA3P1 for 24 hours and then treated with 0.25 μM Dox for 36 hours before DAPI staining or for 30 hours before immunoblotting. (E) Silencing of TRAF6 diminished the inhibitory role of PDIA3P1 on Dox-induced apoptosis. SK-PDIA3P1 and its control cell line SK-Ctrl were transfected with NC or siTRAF6 for 24 hours and then treated with 1 μM Dox for 48 hours before DAPI staining. + or – indicates cells with (+) or without (–) the indicated treatment. For (A), (B), and (D), GAPDH was used as an internal control. For (C) and (D), data are expressed as the mean ± SEM of at least three independent experiments. *$P < 0.05$; **$P < 0.01$; ***$P < 0.001$.

overexpression antagonized the promotive effect of siPDIA3P1 on Dox-induced apoptosis (Fig. 4D), whereas silencing TRAF6 abrogated the inhibitory effect of PDIA3P1 on Dox-induced apoptosis (Fig. 4E). These results indicate that PDIA3P1 may enhance Dox-induced NF-κB activation and in turn promote tumor cell survival by enhancing TRAF6 expression.

To explore how PDIA3P1 up-regulated TRAF6, we first examined the subcellular localization of PDIA3P1 and found that PDIA3P1 was located primarily in the cytoplasm (Fig. 5A; Supporting Fig. S13A). One of the main working models of cytoplasmic lncRNAs suggests that they act as ceRNAs to bind to miRNA and in turn up-regulate the expression of miRNA targets. Therefore, RIP assays were used to detect the amount of PDIA3P1 in the protein complex precipitated by antibody against AGO2, the key component that is associated with miRNA. Compared with the IgG control group, considerably more PDIA3P1 was detected in the anti-AGO2 precipitates, whereas no enrichment of U6, a negative control RNA, was detected in the AGO2 complex (Fig. 5B), suggesting that PDIA3P1 may interact with AGO2 *in vivo*. Moreover, silencing of DROSHA or DICER1, the molecules critical for miRNA biogenesis, abrogated the siPDIA3P1-induced down-regulation of TRAF6 (Fig. 5C; Supporting Fig. S13B). These data indicate
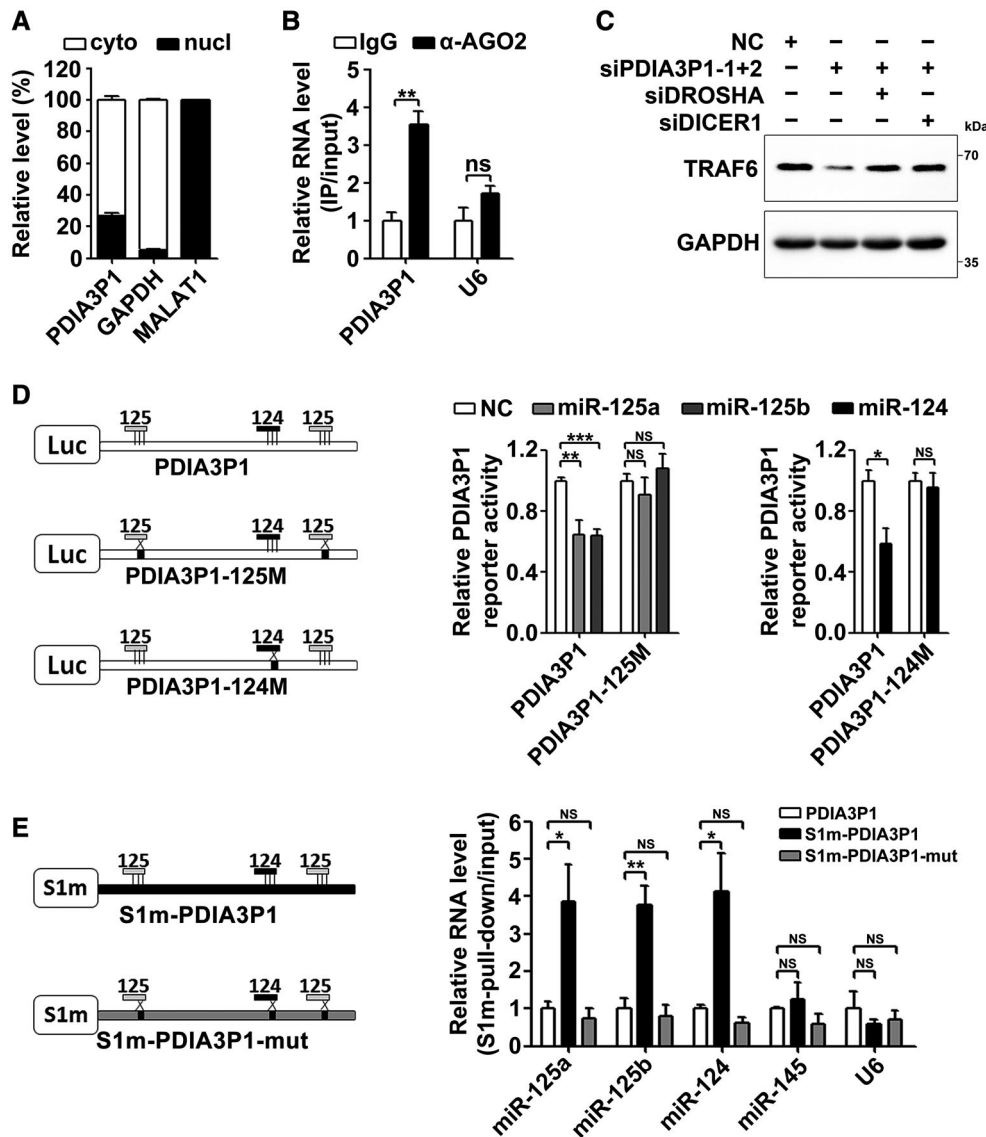
FIG. 5. PDIA3P1 interacts with miR-125a/b and miR-124. (A) PDIA3P1 was localized primarily in the cytoplasm. The cytoplasm and nucleus of SK-Hep-1 cells were isolated and then subjected to RNA extraction and real-time quantitative PCR analysis for the indicated genes. GAPDH and lncRNA MALAT1 (metastasis-associated lung adenocarcinoma transcript 1) were used as the controls for cytoplasmic (cyto) and nuclear (nucl) fraction, respectively. (B) PDIA3P1 interacted with AGO2 *in vivo*. QGY-7703 cells were subjected to RIP assays with an AGO2 antibody or isotype-matched control IgG. The RNA levels of PDIA3P1 or U6 in the anti-AGO2 precipitates, IgG precipitates, and input were analyzed by real-time quantitative PCR. The RNA level in the antibody precipitates was adjusted by that in the input. The mean value of the adjusted RNA level in the IgG precipitates from three experiments was set as relative RNA level 1. U6 was used as a negative control. (C) Silencing of DROSHA or DICER1 rescued the siPDIA3P1-induced reduction in the TRAF6 level. SK-Hep-1 cells were co-transfected with the indicated siRNA duplexes for 48 hours before immunoblotting. GAPDH was used as an internal control; + or – indicates cells with (+) or without (–) the indicated treatment. (D) Ectopic expression of miR-125a/b or miR-124 suppressed the activity of firefly luciferase containing the miR-125a/b or miR-124 binding sequences of PDIA3P1. The short vertical lines in the schematic diagram indicate the target sites of miR-125a/b and miR-124 in PDIA3P1, whereas the crosses depict the mutated sites in PDIA3P1-125M and PDIA3P1-124M (left panel). SK-Hep-1 cells were co-transfected with NC or miR-125a/b, pRL-PGK, and pGL3cm-PDIA3P1 or pGL3cm-PDIA3P1-125M (middle panel), or co-transfected with NC or miR-124, pRL-PGK, and pGL3cm-PDIA3P1 or pGL3cm-PDIA3P1-124M (right panel). Luciferase activity was detected 48 hours after transfection. (E) PDIA3P1 physically interacted with cellular miR-125a/b and miR-124. The short vertical lines in the schematic diagram indicate the target sites of miR-125a/b and miR-124 in S1m-PDIA3P1, whereas the crosses depict the mutated sites in S1m-PDIA3P1-mut (left panel). The QGY-PDIA31P1, QGY-S1m-PDIA3P1, and QGY-S1m-PDIA3P1-mut sublines were subjected to S1m-tagged RNA affinity purification (right panel). The RNA levels in the S1m-pull-down product and the input were analyzed by real-time quantitative PCR. The RNA level in the pull-down product was adjusted by that in the input. The mean value of the adjusted RNA level in the pull-down product of the QGY-PDIA3P1 group from three experiments was set as relative RNA level 1. miR-145 and U6 were used as negative controls. For (B), (D), and (E), data are expressed as the mean ± SEM of at least three independent experiments. *P < 0.05; **P < 0.01; ***P < 0.001.

that PDIA3P1 may enhance TRAF6 expression in a miRNA-dependent manner.

Subsequent bioinformatics analyses with TargetScan identified putative binding sites of miR-125a/b and miR-124 in both PDIA3P1 (Supporting Fig. S13C) and the 3′ UTR of TRAF6 (Supporting Fig. S13D). Further analysis using a dual-luciferase reporter system revealed that overexpression of miR-125a/b or miR-124 significantly reduced the activity of firefly luciferase carrying full-length PDIA3P1, and this effect was abrogated when the predicted miR-125a/b or miR-124 binding site in PDIA3P1 was mutated (Fig. 5D; Supporting Fig. S14A). To further demonstrate the physical interaction between PDIA3P1 and miR-125a/b/124, the full-length PDIA3P1 that contained wild-type or mutant miR-125a/b or miR-124 binding sequences was tagged with a modified streptavidin-binding RNA aptamer S1m (Fig. 5E, left panel). Hepatoma cells with stable expression of S1m-PDIA3P1, S1m-PDIA3P1-mut, or untagged PDIA3P1 were subjected to RNA affinity purification using streptavidin beads. As expected, PDIA3P1 was enriched in the precipitates from S1m-PDIA3P1 and S1m-PDIA3P1 mut-transfected cells compared with those from untagged-PDIA3P1 transfectants, whereas no enrichment of 18S ribosomal RNA, the negative control, was observed (Supporting Fig. S14B). Compared with the untagged-PDIA3P1 group,

miR-125a/b and miR-124 were significantly enriched in the S1m-PDIA3P1 but not S1m-PDIA3P1-mut precipitates, and no enrichment of the negative controls, miR-145 and U6, was detected in any precipitates (Fig. 5E). In addition, overexpression of miR-125a/b and miR-124 did not affect PDIA3P1 expression (Supporting Fig. S14C). These results suggest that PDIA3P1 may physically interact with miR-125a/b and miR-124 *in vivo*, and miR-125a/b and miR-124 may not affect the RNA stability of PDIA3P1.

Next, we examined whether miR-125a/b and miR-124 directly bound to TRAF6 and regulated its expression. A dual-luciferase reporter assay showed that overexpression of miR-125a/b or miR-124 significantly reduced the activity of firefly luciferase with TRAF6-3′ UTR (Fig. 6A; Supporting Fig. S15A) and diminished the level of cellular TRAF6 protein (Fig. 6B; Supporting Fig. S15B). Furthermore, PDIA3P1 knockdown abated the activity of firefly luciferase containing TRAF6-3′ UTR (Fig. 6C; Supporting Fig. S15C), which mimicked the effect of miR-125a/b and miR-124 overexpression. In contrast, PDIA3P1 overexpression attenuated the function of miR-125a/b or miR-124 in decreasing the activity of luciferase with TRAF6-3′ UTR (Fig. 6D; Supporting Fig. S15D). Consistently, the role of siPDIA3P1 in reducing the TRAF6 protein level was abrogated by antagonizing cellular miR-125 or miR-124 (Fig. 6E;
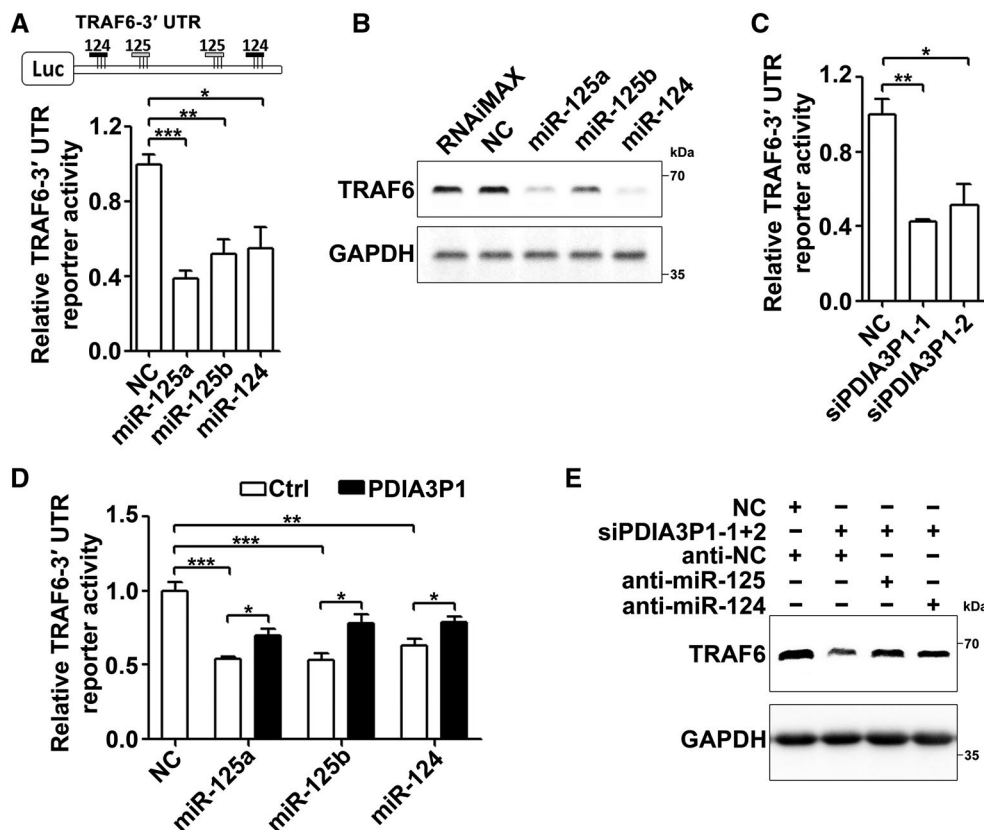
FIG. 6. PDIA3P1 relieves the repression of miR-125a/b/miR-124 on TRAF6. (A) miR-125a/b and miR-124 suppressed the activity of firefly luciferase containing the miR-125a/b or miR-124 binding sequences of TRAF6-3′ UTR. The short vertical lines in the schematic diagram indicate the target sites of miR-125a/b and miR-124 in TRAF6-3′ UTR (upper panel). SK-Hep-1 cells were co-transfected with the indicated RNA duplex, pRL-PGK, and pGL3cm-TRAF6-3′ UTR for 48 hours before luciferase activity analysis. (B) Ectopic expression of miR-125a/b or miR-124 decreased the protein level of TRAF6. SK-Hep-1 cells were transfected with the indicated RNA duplexes for 48 hours before immunoblotting. RNAiMAX indicates cells exposed to Lipofectamine RNAiMAX but not RNA duplexes. (C) PDIA3P1 knockdown suppressed the TRAF6-3′ UTR reporter activity. SK-Hep-1 cells were transfected with NC or siPDIA3P1 for 24 hours, followed by co-transfection with pRL-PGK and pGL3cm-TRAF6-3′ UTR for 48 hours before luciferase activity analysis. (D) PDIA3P1 overexpression attenuated the function of miR-125a/b and miR-124 in decreasing the TRAF6-3′ UTR reporter activity. SK-PDIA3P1 and its control line SK-Ctrl were co-transfected with the indicated RNA duplexes, pRL-PGK, and pGL3cm-TRAF6-3′ UTR for 48 hours before luciferase activity analysis. (E) Antagonism of cellular miR-125a/b or miR-124 rescued the siPDIA3P1-induced reduction in the TRAF6 level. SK-Hep-1 cells were co-transfected with the indicated siRNA duplexes and miRNA inhibitors for 48 hours before immunoblotting. GAPDH was used as an internal control. For (A), (C), and (D), data are expressed as the mean ± SEM of at least three independent experiments. *$P < 0.05$; **$P < 0.01$; ***$P < 0.001$.

Supporting Fig. S15E). Consistent with these findings, PDIA3P1 up-regulation was significantly correlated with elevation of TRAF6 or phosphorylated-NF-κB/p65 in human HCC tissues (Fig. 7A,B). However, no correlation between the levels of PDIA3P1 and miR-125a/b or miR-124 was observed (Supporting Fig. S16).

Taken together, PDIA3P1 may up-regulate TRAF6 expression by serving as a ceRNA to bind miR-125a/b and miR-124.

DOX TREATMENT PREVENTS THE hMTR4-MEDIATED DOWN-REGULATION OF PDIA3P1

To explore the mechanisms underlying Dox-induced up-regulation of PDIA3P1, cells were transfected with a luciferase reporter p-(−2,129/+358) that contained the −2,129 base pairs (bp) ~ +358 bp region of PDIA3P1. Increased luciferase activity was observed in p-(−2,129/+358) transfectants, but the
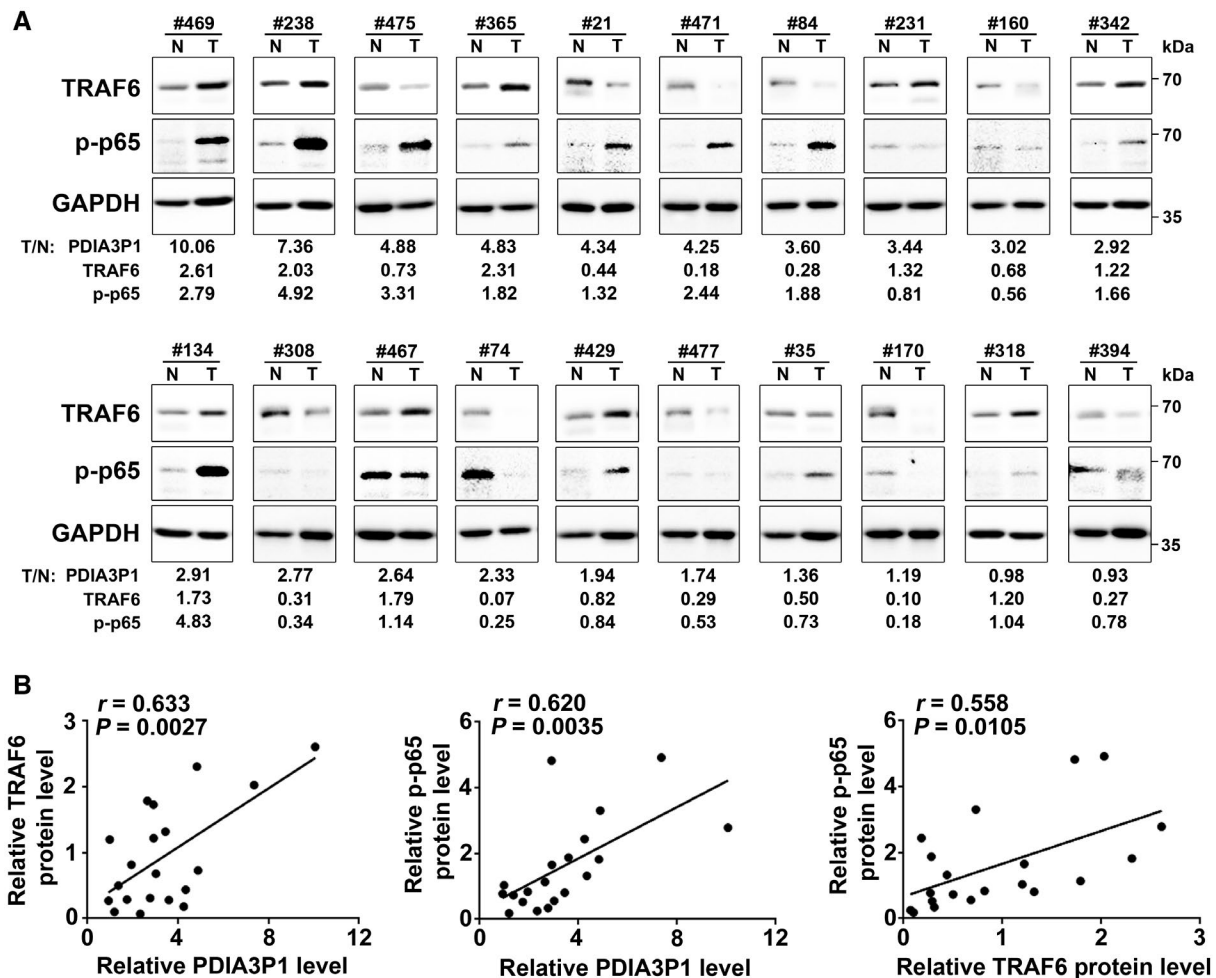
FIG. 7. Positive correlation between up-regulation of PDIA3P1 and elevation of TRAF6 or phosphorylated-NF-κB/p-p65 in human HCC tissues. (A) Detection of PDIA3P1, TRAF6, and phosphorylated-NF-κB/p-p65 in paired HCC and adjacent nontumor livers. PDIA3P1 expression was analyzed by real-time quantitative PCR. TRAF6 and phosphorylated-NF-κB/p-p65 were detected by immunoblotting, and the intensity of each band was quantified. The values under each pair of samples (T/N) indicate the level of the indicated molecules in HCC tissue (T) relative to that of corresponding nontumor liver (N). (B) PDIA3P1 up-regulation was correlated with the increase of TRAF6 or phosphorylated-NF-κB/p65. The correlation was determined using the Pearson correlation coefficient, based on the expression data from (A).

promoter activity was not enhanced after Dox exposure (Supporting Fig. S17A). In addition, IL-1β or TNFα did not increase the expression of PDIA3P1 (Supporting Fig. S17B), indicating that PDIA3P1 is not transactivated by NF-κB, and the Dox-induced up-regulation of PDIA3P1 may not result from increased transcription.

RNA-binding proteins (RBPs) are key posttranscriptional regulators of RNA expression.[19] To explore whether RBPs play a role in Dox-induced PDIA3P1 expression, an RNA pull-down assay was conducted. hMTR4, a superkiller-2-like RNA helicase that is encoded by *SKIV2L2* and promotes RNA degradation by RNA exosome,[20] was identified in the protein complexes pulled down by PDIA3P1 but not in those pulled down by the antisense RNA of PDIA3P1 (AS-PDIA3P1, used as a negative control) (Supporting Fig. S18A-C; Fig. 8A). The negative control glyceraldehyde 3-phosphate dehydrogenase (GAPDH) was not detected in either PDIA3P1 or AS-PDIA3P1 precipitated proteins (Fig. 8A; Supporting Fig. S18C). The *in vivo* interaction between PDIA3P1 and hMTR4 was confirmed by RIP assay using hMTR4 antibody. Compared with
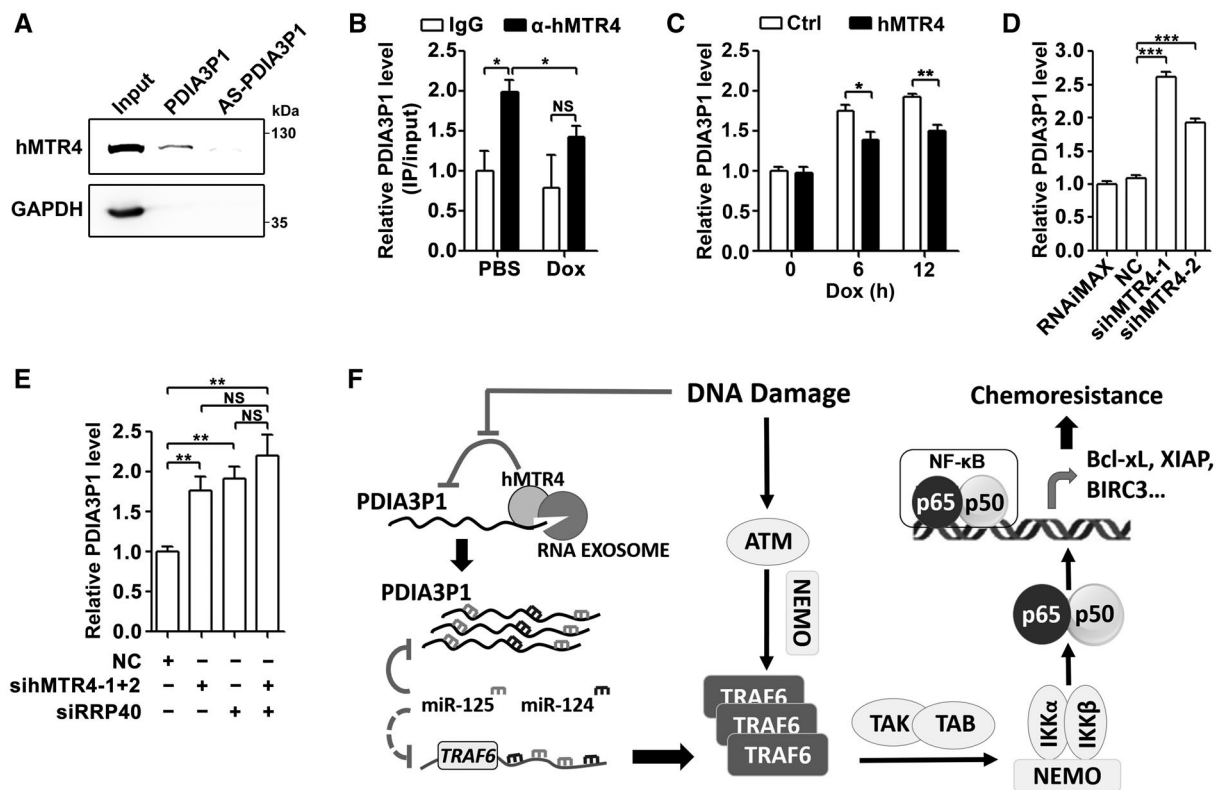
FIG. 8. Dox treatment prevents hMTR4-mediated down-regulation of PDIA3P1. (A) hMTR4 was enriched in the PDIA3P1 pull-down complexes. The cellular proteins in SK-Hep-1 cells were pulled down with biotinylated PDIA3P1 or its antisense RNA (AS-PDIA3P1, as negative control) and then subjected to immunoblotting. (B) The interaction between hMTR4 and PDIA3P1 was diminished following Dox treatment. SK-Hep-1 cells were incubated in the presence of vehicle (PBS) or 1 μM Dox for 9 hours before RIP assays with an hMTR4 antibody or isotype-matched control IgG. The RNA levels of PDIA3P1 in the anti-hMTR4 precipitates, IgG precipitates, and input were analyzed. The RNA level in the antibody precipitates was adjusted by that in the input. The mean value of the adjusted RNA level in the IgG precipitates of vehicle group from four experiments was set as relative RNA level 1. (C) Ectopic expression of hMTR4 attenuated the Dox-triggered PDIA3P1 increase. QGY-hMTR4 or its control cell line QGY-Ctrl was incubated with 1 μM Dox for the indicated hours before real-time quantitative PCR analysis. (D) Silencing of hMTR4 increased the PDIA3P1 level. SK-Hep-1 cells were transfected with the indicated RNA duplexes for 48 hours before real-time quantitative PCR analysis. (E) Effect of RRP40 and/or hMTR4 knockdown on the expression of PDIA3P1. SK-Hep-1 cells were co-transfected with the indicated siRNA duplexes for 48 hours before real-time quantitative PCR analysis; + or – indicates cells with (+) or without (–) the indicated treatment. For (A), (C)-(E), GAPDH was used as an internal control. For (B)-(E), data are expressed as the mean ± SEM of at least three independent experiments. *$P < 0.05$; **$P < 0.01$; ***$P < 0.001$. (F) Model of the hMTR4-PDIA3P1-miR-125a/b/124-TRAF6 axis and its role in DNA damage-induced activation of NF-κB signaling.

the IgG-bound complex, a significant enrichment of PDIA3P1 RNA was detected in the anti-hMTR4 precipitates, whereas Dox treatment significantly attenuated the enrichment of PDIA3P1 in the hMTR4 complexes (Fig. 8B). However, the circular RNA of homeodomain-interacting protein kinase 3 (circHIPK3), a negative control, was not enriched in the hMTR4 complexes (Supporting Fig. S18D). In addition, the protein level of hMTR4 did not change following Dox treatment (Supporting Fig. S19A). These results suggest that hMTR4 is associated with

PDIA3P1, and this association may be disrupted by Dox treatment. Consistently, overexpression of hMTR4 (Supporting Fig. S19B) prevented Dox-induced PDIA3P1 accumulation (Fig. 8C), whereas silencing of hMTR4 increased the PDIA3P1 level (Fig. 8D; Supporting Fig. S20). Moreover, silencing of RRP40, a core component of the RNA exosome, significantly increased the PDIA3P1 level (Fig. 8E), which mimicked the effect of hMTR4 silencing. However, simultaneous suppression of hMTR4 and RRP40 did not further increase the PDIA3P1 level

(Fig. 8E). These results suggest that hMTR4 may abrogate Dox-induced PDIA3P1 accumulation by activating the RNA exosome.

Taken together, our results suggest that DNA-damaging agents, such as Dox, may decrease the association between hMTR4 and PDIA3P1 and abrogate RNA exosome-mediated PDIA3P1 degradation. The resulting increased PDIA3P1 may act as an endogenous sponge of miR-125a/b and miR-124 to up-regulate TRAF6 expression, leading to NF-κB activation and resistance of tumor cells to DNA-damaging agents (Fig. 8F).

Discussion

DNA damage-induced NF-κB activation is a major impediment to effective antitumor chemotherapy.[21] Therefore, it is of clinical significance to identify new molecules in the NF-κB pathway that may be targeted to increase chemosensitivity. In addition to regulatory proteins and microRNAs, lncRNA is emerging as another critical player in the control of NF-κB signaling.

In this report, we identified PDIA3P1 as a regulator of the NF-κB pathway and chemosensitivity based on the following evidence: (1) PDIA3P1 was up-regulated in different types of cancer and in response to DNA-damaging agents; (2) silencing of PDIA3P1 significantly attenuated Dox-induced activation of NF-κB signaling, promoted Dox-induced apoptosis *in vitro*, and sensitized tumor xenografts to Dox treatment *in vivo*, whereas overexpression of PDIA3P1 abrogated Dox-induced apoptosis and desensitized xenografts to Dox treatment; (3) the promotive effect of siPDIA3P1 on Dox-induced apoptosis was antagonized by either IκB knockdown or TRAF6 overexpression, and administration of BAY 11-7085, an NF-κB inhibitor, attenuated the PDIA3P1-induced resistance to Dox treatment in mouse xenografts; and (4) a significant correlation between up-regulation of PDIA3P1 and elevation of TRAF6, phosphoralated-p65, or NF-κB downstream anti-apoptosis genes was observed in human HCC tissues. These data indicate that PDIA3P1 up-regulation may confer chemoresistance, and targeting PDIA3P1 represents a promising strategy to inactivate NF-κB signaling and enhance the chemosensitivity of cancer cells.

TRAF6 is an essential intermediate in the NF-κB signaling pathway, and it can be activated by various stimuli, including DNA damage.[14,22] The activity and expression of TRAF6 is tightly regulated. Activation of TRAF6 requires K63-linked polyubiquitination, and removing the K63-linked ubiquitin chains from TRAF6 terminates NF-κB signaling.[23,24] On the other hand, K48-linked polyubiquitination-mediated degradation and miRNA-mediated suppression are important mechanisms by which the protein level of TRAF6 is regulated.[25-27] Here, we identified a mechanism of TRAF6 expression regulation that was mediated by noncoding RNA: miR-125a/b and miR-124 suppressed the expression of TRAF6, whereas PDIA3P1 enhanced the TRAF6 protein level by acting as a ceRNA to bind miR-125a/b/miR-124 and relieve their repression on TRAF6. miR-125a/b and miR-124, which have implications in various cell activities, are both down-regulated in HCC cells and act as tumor suppressors in liver cancer.[28-30] Because PDIA3P1 bears binding sites for both miR-125a/b and miR-124, it may also play an oncogenic role by titrating these miRNAs and regulating signaling pathways other than the NF-κB pathway.

The RNA exosome is an evolutionarily conserved ribonucleolytic complex that mediates RNA processing and degradation.[20] It consists of catalytic subunits and a nine-subunit core (Exo9) that contains RRP40.[31] Cofactors that associate with the RNA exosome dictate its substrate specificity. hMTR4 is a prominent cofactor of the RNA exosome and promotes exosome-mediated RNA degradation.[32,33] The trimeric nuclear exosome targeting (NEXT) complex, which contains hMTR4, RNA-binding motif protein 7 (RBM7), and zinc finger CCHC-type containing 8, is responsible for the degradation of the promoter upstream transcripts (PROMPTs).[32,34,35] Moreover, silencing of the exosome core component RRP40 or its cofactor hMTR4 causes accumulation of both mRNAs and lncRNAs.[35] It has been shown that ultraviolet -induced DNA damage attenuates the interaction of NEXT complex with the PROMPTs by phosphorylating RBM7, which consequently increases the level of PROMPTs,[36] indicating that exosome-mediated RNA turnover can be altered following DNA damage. Consistently, we observed that Dox treatment also decreased the binding of hMTR4 with PDIA3P1 as well as three

representative PROMPTs, including the promoter upstream transcripts of serine/threonine kinase 11 interacting protein (proSTK11IP), pogo transposable element derived with ZNF domain (proPOGZ), and growth arrest and DNA-damage-inducible 45 alpha (proGADD45a) (Supporting Fig. S21). Furthermore, hMTR4 or RRP40 knockdown significantly increased the PDIA3P1 level, whereas hMTR4 overexpression attenuated Dox-induced increase in the PDIA3P1 level. These data indicate the general involvement of hMTR4 and the RNA exosome in posttranscriptional regulation of lncRNA expression and in cell response to DNA damage.

In summary, we identify a hMTR4-PDIA3P1-miR-125/124-TRAF6 regulatory axis and elucidate its function in DNA damage-activated NF-κB signaling, which may be exploited for anticancer therapy. We show the promoting effects of PDIA3P1 in TRAF6 expression and NF-κB signaling, characterize the ceRNA function of PDIA3P1, reveal the regulatory role of hMTR4 on PDIA3P1 expression, and disclose the significance of targeting PDIA3P1 in enhancing tumor chemosensitivity.

Author Contributions: C.X. was responsible for the study design, implementation of the experiments, interpretation of the data, and drafting of the manuscript. L.-Z.Z., Z.-L.C., W.-J.Z., M.-H.X., and N.Z. were responsible for implementation of the experiments and interpretation of the data. J.-H.F. and Y.Z. were responsible for the study design and interpretation of the data. Z.-W.G. and X.H. were responsible for the bioinformatics analyses. S.-M.Z. was responsible for supervision of the project, study design, interpretation of the data, and drafting of the manuscript.

REFERENCES

1) Quinn JJ, Chang HY. Unique features of long non-coding RNA biogenesis and function. Nat Rev Genet 2016;17:47-62.

2) Chen LL. Linking long noncoding RNA localization and function. Trends Biochem Sci 2016;41:761-772.

3) Tseng YY, Moriarity BS, Gong W, Akiyama R, Tiwari A, Kawakami H, et al. PVT1 dependence in cancer with MYC copy-number increase. Nature 2014;512:82-86.

4) Song Y, Liu C, Liu X, Trottier J, Beaudoin M, Zhang L, et al. H19 promotes cholestatic liver fibrosis by preventing ZEB1-mediated inhibition of epithelial cell adhesion molecule. HEPATOLOGY 2017;66:1183-1196.

5) Liu B, Sun L, Liu Q, Gong C, Yao Y, Lv X, et al. A cytoplasmic NF-kappaB interacting long noncoding RNA blocks IkappaB phosphorylation and suppresses breast cancer metastasis. Cancer Cell 2015;27:370-381.

6) **Zhang J**, **Li Z**, **Liu L**, Wang Q, Li S, Chen D, et al. Long non-coding RNA TSLNC8 is a tumor suppressor that inactivates the interleukin-6/STAT3 signaling pathway. HEPATOLOGY 2018;67: 171-187.

7) Lee S, Kopp F, Chang TC, Sataluri A, Chen B, Sivakumar S, et al. Noncoding RNA NORAD regulates genomic stability by sequestering PUMILIO proteins. Cell 2016;164:69-80.

8) Yuan JH, Yang F, Wang F, Ma JZ, Guo YJ, Tao QF, et al. A long noncoding RNA activated by TGF-β promotes the invasion-metastasis cascade in hepatocellular carcinoma. Cancer Cell 2014;25:666-681.

9) Hosono Y, Niknafs YS, Prensner JR, Iyer MK, Dhanasekaran SM, Mehra R, et al. Oncogenic role of THOR, a conserved cancer/testis long non-coding RNA. Cell 2017;171:1559-1572.

10) Yoon JH, Abdelmohsen K, Srikantan S, Yang X, Martindale JL, De S, et al. LincRNA-p21 suppresses target mRNA translation. Mol Cell 2012;47:648-655.

11) Taniguchi K, Karin M. NF-κB, inflammation, immunity and cancer: coming of age. Nat Rev Immunol 2018;18:309-324.

12) Zhang B, Zhang Z, Li L, Qin Y-R, Liu H, Jiang C, et al. TSPAN15 interacts with BTRC to promote oesophageal squamous cell carcinoma metastasis via activating NF-κB signaling. Nat Commun 2018;9:1423.

13) Zhang Q, Lenardo MJ, Baltimore D. 30 years of NF-kappaB: a blossoming of relevance to human pathobiology. Cell 2017;168: 37-57.

14) Napetschnig J, Wu H. Molecular basis of NF-κB signaling. Annu Rev Biophys 2013;42:443-468.

15) Hinz M, Scheidereit C. The IκB kinase complex in NF-κB regulation and beyond. EMBO Rep 2013;15:46-61.

16) Jin C, Jia L, Huang Y, Zheng Y, Du N, Liu Y, et al. Inhibition of lncRNA MIR31HG promotes osteogenic differentiation of human adipose-derived stem cells. Stem Cells 2016;34:2707-2720.

17) Rapicavoli NA, Qu K, Zhang J, Mikhail M, Laberge RM, Chang HY. A mammalian pseudogene lncRNA at the interface of inflammation and anti-inflammatory therapeutics. ELife 2013;2: e00762.

18) Su H, Yang JR, Xu T, Huang J, Xu L, Yuan Y, et al. MicroRNA-101, down-regulated in hepatocellular carcinoma, promotes apoptosis and suppresses tumorigenicity. Cancer Res 2009;69:1135-1142.

19) Gerstberger S, Hafner M, Tuschl T. A census of human RNA-binding proteins. Nat Rev Genet 2014;15:829-845.

20) Kilchert C, Wittmann S, Vasiljeva L. The regulation and functions of the nuclear RNA exosome complex. Nat Rev Mol Cell Biol 2016;17:227-239.

21) Roos WP, Thomas AD, Kaina B. DNA damage and the balance between survival and death in cancer biology. Nat Rev Cancer 2016;16:20-33.

22) Hinz M, Stilmann M, Arslan SÇ, Khanna KK, Dittmar G, Scheidereit C. A cytoplasmic ATM-TRAF6-cIAP1 module links

nuclear DNA damage signaling to ubiquitin-mediated NF-κB activation. Mol Cell 2010;40:63-74.

23) **Boone DL**, **Turer EE**, **Lee EG**, Ahmad RC, Wheeler MT, Tsui C, et al. The ubiquitin-modifying enzyme A20 is required for termination of Toll-like receptor responses. Nat Immunol 2004;5:1052-1060.

24) Kovalenko A, Chable-Bessia C, Cantarella G, Israël A, Wallach D, Courtois G. The tumour suppressor CYLD negatively regulates NF-κB signalling by deubiquitination. Nature 2003;424:801-805.

25) Zhao W, Wang L, Zhang M, Yuan C, Gao C. E3 ubiquitin ligase tripartite motif 38 negatively regulates TLR-mediated immune responses by proteasomal degradation of TNF receptor-associated factor 6 in macrophages. J Immunol 2012;188:2567-2574.

26) Zhou X, Liu Z, Cheng X, Zheng Y, Zeng F, He Y. Socs1 and Socs3 degrades Traf6 via polyubiquitination in LPS-induced acute necrotizing pancreatitis. Cell Death Dis 2015;6:e2012.

27) Zhang X, Zhu C, Wang T, Jiang H, Ren Y, Zhang Q, et al. GP73 represses host innate immune response to promote virus replication by facilitating MAVS and TRAF6 degradation. PLoS Pathog 2017;13:e1006321.

28) Kim JK, Noh JH, Jung KH, Eun JW, Bae HJ, Kim MG, et al. Sirtuin7 oncogenic potential in human hepatocellular carcinoma and its regulation by the tumor suppressors MiR-125a-5p and MiR-125b. HEPATOLOGY 2013;57:1055-1067.

29) Gong J, Zhang J, Li B, Zeng C, You K, Chen MX, et al. MicroRNA-125b promotes apoptosis by regulating the expression of Mcl-1, Bcl-w and IL-6R. Oncogene 2013;32:3071-3079.

30) Zheng F, Liao YJ, Cai MY, Liu YH, Liu TH, Chen SP, et al. The putative tumour suppressor microRNA-124 modulates hepatocellular carcinoma cell aggressiveness by repressing ROCK2 and EZH2. Gut 2012;61:278-289.

31) Zinder JC, Lima CD. Targeting RNA for processing or destruction by the eukaryotic RNA exosome and its cofactors. Gene Dev 2017;31:88-100.

32) **Lubas M**, **Christensen MS**, **Kristiansen MS**, Domanski M, Falkenby LG, Lykke-Andersen S, et al. Interaction profiling identifies the human nuclear exosome targeting complex. Mol Cell 2011;43:624-637.

33) **Meola N**, **Domanski M**, Karadoulama E, Chen Y, Gentil C, Pultz D, et al. Identification of a nuclear exosome decay pathway for processed transcripts. Mol Cell 2016;64:520-533.

34) Pascal P, Jesper N, Susanne K, SøRen LA, Christensen MS, Mapendano CK, et al. RNA exosome depletion reveals transcription upstream of active human promoters. Science 2008;322:1851-1854.

35) **Fan J**, **Kuai B**, Wu G, Wu X, Chi B, Wang L, et al. Exosome cofactor hMTR4 competes with export adaptor ALYREF to ensure balanced nuclear RNA pools for degradation and export. EMBO J 2017;36:2870-2886.

36) Blasius M, Wagner SA, Choudhary C, Bartek J, Jackson SP. A quantitative 14-3-3 interaction screen connects the nuclear exosome targeting complex to the DNA damage response. Gene Dev 2014;28:1977-1982.

Author names in bold designate shared co-first authorship.

Supporting Information